Heterogeneous lithium niobate photonics on silicon substrates

Payam Rabiei,[1,*] Jichi Ma,[1] Saeed Khan,[1,2] Jeff Chiles,[1] and Sasan Fathpour[1,2,3]

[1]*CREOL, The College of Optics and Photonics, Bldg. 53, University of Central Florida, 4000 Central Florida Blvd., Orlando, FL 32816, USA*

[2]*Department of Electrical and Computer Engineering, University of Central Florida, 4000 Central Florida Blvd., Orlando, FL 32816, USA*

[3]*fathpour@creol.ucf.edu*

**pr@partow-tech.com*

Abstract: A platform for the realization of tightly-confined lithium niobate photonic devices and circuits on silicon substrates is reported based on wafer bonding and selective oxidation of refractory metals. The heterogeneous photonic platform is employed to demonstrate high-performance lithium niobate microring optical resonators and Mach-Zehnder optical modulators. A quality factor of ~7.2×10^4 is measured in the microresonators, and a half-wave voltage-length product of 4 V.cm and an extinction ratio of 20 dB is measured in the modulators.

OCIS codes: (130.0130) Integrated optics; (230.4000) Microstructure fabrication; (230.5750) Resonators; (130.4110) Modulators.

References and links

1. B. Jalali and S. Fathpour, "Silicon photonics," J. Lightwave Technol. **24**(12), 4600–4615 (2006).
2. A. W. Fang, H. Park, O. Cohen, R. Jones, M. J. Paniccia, and J. E. Bowers, "Electrically pumped hybrid AlGaInAs-silicon evanescent laser," Opt. Express **14**(20), 9203–9210 (2006).
3. J. Yang, Z. Mi, and P. Bhattacharya, "Groove-coupled InGaAs/GaAs quantum dot laser/waveguide on silicon," J. Lightwave Technol. **25**(7), 1826–1831 (2007).
4. M. J. Weber, *Handbook of Optical Materials* (CRC Press, 2003).
5. R. Brinkmann, I. Baumann, M. Dinand, W. Sohler, and H. Suche, "Erbium-doped single- and double-pass Ti:$LiNbO_3$ waveguide amplifiers," IEEE J. Quantum Electron. **30**(10), 2356–2360 (1994).
6. R. S. Jacobsen, K. N. Andersen, P. I. Borel, J. Fage-Pedersen, L. H. Frandsen, O. Hansen, M. Kristensen, A. V. Lavrinenko, G. Moulin, H. Ou, C. Peucheret, B. Zsigri, and A. Bjarklev, "Strained silicon as a new electro-optic material," Nature **441**(7090), 199–202 (2006).
7. K. K. Tsia, S. Fathpour, and B. Jalali, "Electrical tuning of birefringence in silicon waveguides," Appl. Phys. Lett. **92**(6), 061109 (2008).
8. G. D. Miller, R. G. Batchko, W. M. Tulloch, D. R. Weise, M. M. Fejer, and R. L. Byer, "42%-efficient single-pass cw second-harmonic generation in periodically poled lithium niobate," Opt. Lett. **22**(24), 1834–1836 (1997).
9. S. Tanzilli, H. D. Riedmatten, W. Tittle, H. Zbinden, P. Baldi, M. D. Micheli, D. B. Ostrowsky, and N. Gisin, "Highly efficient photon-pair source using periodically poled lithium niobate waveguide," Electron. Lett. **37**(1), 26–28 (2001).
10. Y.-S. Lee, T. Meade, V. Perlin, H. Winful, T. B. Norris, and A. Galvanauskas, "Generation of narrow-band terahertz radiation via optical rectification of femtosecond pulses in periodically poled lithium niobate," Appl. Phys. Lett. **76**(18), 2505–2507 (2000).
11. P. Tournois, "Acousto-optic programmable dispersive filter for adaptive compensation of group delay time dispersion in laser systems," Opt. Commun. **140**(4-6), 245–249 (1997).
12. E. L. Wooten, K. M. Kissa, A. Yi-Yan, E. J. Murphy, D. A. Lafaw, P. F. Hallemeier, D. Maack, D. V. Attanasio, D. J. Fritz, G. J. McBrien, and D. E. Bossi, "A review of lithium niobate modulators for fiber-optic communications systems," IEEE J. Sel. Top. Quantum Electron. **6**(1), 69–82 (2000).
13. A. Chiba, T. Sakamoto, T. Kawanishi, K. Higuma, M. Sudo, and J. Ichikawa, "16-level quadrature amplitude modulation by monolithic quad-parallel Mach-Zehnder optical modulator," Electron. Lett. **46**(3), 220–222 (2010).
14. M. De Micheli, J. Botineau, S. Neveu, P. Sibillot, D. B. Ostrowsky, and M. Papuchon, "Independent control of index and profiles in proton-exchanged lithium niobate guides," Opt. Lett. **8**(2), 114–115 (1983).

#196230 - $15.00 USD Received 22 Aug 2013; revised 7 Oct 2013; accepted 8 Oct 2013; published 18 Oct 2013

15. R. C. Alferness, V. Ramaswamy, S. Korotky, M. Divino, and L. Buhl, "Efficient single-mode fiber to titanium diffused lithium niobate waveguide coupling for λ = 1.32 μm," IEEE J. Quantum Electron. **18**(10), 1807–1813 (1982).
16. Y. S. Lee, G. D. Kim, W. J. Kim, S. S. Lee, W. G. Lee, and W. H. Steier, "Hybrid Si-$LiNbO_3$ microring electro-optically tunable resonators for active photonic devices," Opt. Lett. **36**(7), 1119–1121 (2011).
17. L. Chen and R. M. Reano, "Compact electric field sensors based on indirect bonding of lithium niobate to silicon microrings," Opt. Express **20**(4), 4032–4038 (2012).
18. I. Bakish, R. Califa, T. Ilovitsh, V. Artel, G. Winzer, K. Voigt, L. Zimmermann, E. Shekel, C. N. Sukenik, and A. Zadok, "Voltage-Induced Phase Shift in a Hybrid $LiNbO_3$-on-Silicon Mach-Zehnder Interferometer," in *Advanced Photonics 2013*, H. Chang, V. Tolstikhin, T. Krauss, and M. Watts, eds., OSA Technical Digest (online) (Optical Society of America, 2013), paper IW4A.2.
19. P. Rabiei and P. Gunter, "Optical and electro-optical properties of submicrometer lithium niobate slab waveguides prepared by crystal ion slicing and wafer bonding," Appl. Phys. Lett. **85**(20), 4603–4605 (2004).
20. M. Levy, R. M. Osgood, R. Liu, L. E. Cross, G. S. Cargill, A. Kumar, and H. Bakhru, "Fabrication of single-crystal lithium niobate films by crystal ion slicing," Appl. Phys. Lett. **73**(16), 2293 (1998).
21. P. Rabiei and W. H. Steier, "Lithium niobate ridge waveguides and modulators fabricated using smart guide," Appl. Phys. Lett. **86**(16), 161115 (2005).
22. H. Hu, R. Ricken, and W. Sohler, "Lithium niobate photonic wires," Opt. Express **17**(26), 24261–24268 (2009).
23. A. Guarino, G. Poberaj, D. Rezzonico, R. Degl'Innocenti, and P. Günter, "Electro–optically tunable microring resonators in lithium niobate," Nat. Photonics **1**(7), 407–410 (2007).
24. H. Hu, R. Ricken, W. Sohler, and R. B. Wehrspohn, "Lithium niobate ridge waveguides fabricated by wet etching," IEEE Photon. Technol. Lett. **19**(6), 417–419 (2007).
25. P. Rabiei, J. Ma, S. Khan, J. Chiles, and S. Fathpour, "Submicron optical waveguides and microring resonators fabricated by selective oxidation of tantalum," Opt. Express **21**(6), 6967–6972 (2013).
26. C. Chaneliere, J. L. Autran, R. A. B. Devine, and B. Balland, "Tantalum pentoxide (Ta_2O_5) thin films for advanced dielectric applications," Mater. Sci. Eng. Rep. **22**(6), 269–322 (1998).
27. N. Matsumoto and K. Kumabe, "AlGaAs–GaAs semiconductor ring lasers," Jpn. J. Appl. Phys. **16**(8), 1395–1398 (1977).
28. B. E. Little, S. T. Chu, H. A. Haus, J. Foresi, and J.-P. Laine, "Microring resonator channel dropping filters," J. Lightwave Technol. **15**(6), 998–1005 (1997).
29. D. Rafizadeh, J. P. Zhang, S. C. Hagness, A. Taflove, K. A. Stair, S. T. Ho, and R. C. Tiberio, "Waveguide-coupled AlGaAs / GaAs microcavity ring and disk resonators with high f inesse and 21.6-nm f ree spectral range," Opt. Lett. **22**(16), 1244–1246 (1997).
30. P. Rabiei, W. H. Steier, C. Zhang, and L. R. Dalton, "Polymer micro-ring filters and modulators," J. Lightwave Technol. **20**(11), 1968–1975 (2002).
31. J. Kondo, A. Kondo, K. Aoki, M. Imaeda, T. Mori, Y. Mizuno, S. Takastsuji, Y. Kozuka, O. Mitomi, and M. Minakata, "40-Gb/s X-Cut $LiNbO_3$ optical modulator with two-step back-slot structure," J. Lightwave Technol. **20**(12), 2110–2114 (2002).
32. G. T. Reed, G. Mashanovich, F. Y. Gardes, and D. J. Thomson, "Silicon optical modulators," Nat. Photonics **4**(8), 518–526 (2010).

1. Introduction

Several unique properties of silicon allow fabrication of ultra-large-scale integrated electronic circuits with extremely high performance. As a result, silicon has been long established as an ideal material for integrated electronics. To date, no material has been able to play a similar unifying role in integrated photonics. Alternatively, hybrid materials and heterogeneous integration solutions are currently being explored, particularly on silicon substrates for compatibility with microelectronics [1]. For instance, several groups are working on technologies to integrate compound semiconductors on silicon photonic chips [1–3]. III-V compound semiconductor waveguides are not very tightly-confined, and hence, silicon itself has been pursued for passive photonics [1]. However, silicon lacks second-order optical nonlinearity for active photonics and, at telecommunication wavelengths, third-order nonlinear silicon devices typically suffer from nonlinear absorptions at the required high optical intensities. Although complicated carrier sweep-out techniques can be employed, they can only partially alleviate the nonlinear absorption problem [1].

Lithium niobate ($LiNbO_3$) is an ideal material with many interesting properties for integrated photonics. First, it is transparent from the ultraviolet to the infrared range (0.35 to 5.0 μm) of the electromagnetic spectrum [4]. Optical gain can be achieved by doping $LiNbO_3$ crystals with rare earth elements, such as erbium [5]. A unique advantage is the material's strong second-order nonlinear optical properties, which are absent in centrosymmetric

#196230 - $15.00 USD Received 22 Aug 2013; revised 7 Oct 2013; accepted 8 Oct 2013; published 18 Oct 2013

semiconductors, like silicon, and amorphous glasses, or are much weaker in noncentrosymmetric crystals like compound semiconductors (it is noted that applying stress can create small birefringence in silicon waveguides but the effect is very weak [6,7]). The second-order nonlinearity of $LiNbO_3$ allows control of the refractive index of the material via the electro-optic (EO) effect. The nonlinearity also allows mixing of optical signals at different wavelengths for parametric amplification, second-harmonic generation, wavelength conversion [8], as well as generation of entangled photon pairs [9]. Even efficient generation of terahertz-frequency signals is reported in the material [10]. Using the piezo-electric properties of $LiNbO_3$, it is possible to make various acousto-optical devices [11]. The most widely used devices based on $LiNbO_3$, meanwhile, are high-speed EO modulators [12]. Extremely high optical modulation performance is possible using the material, since it allows pure phase modulation with virtually no variation in optical absorption. This feature allows vector signal modulation with negligible chirping for advanced telecommunication and other applications [13].

Future applications of $LiNbO_3$ as an integrated optical platform requires a technology that can materialize ultracompact and efficient optical circuits on the material. $LiNbO_3$ optical waveguides are generally very bulky in microphotonic standards and cannot be sharply bent (see Fig. 1). For example, a typical $LiNbO_3$ modulator is 4-5 cm long and tens of micrometers wide [12]. Also, for nonlinear optical applications, due to the low intensity of the pump source in the large cross-sectional optical waveguides, the devices must be a few centimeters long in order to achieve high efficiencies [8,9]. These shortcomings have made $LiNbO_3$ less attractive for integrated photonics, compared to semiconductors.

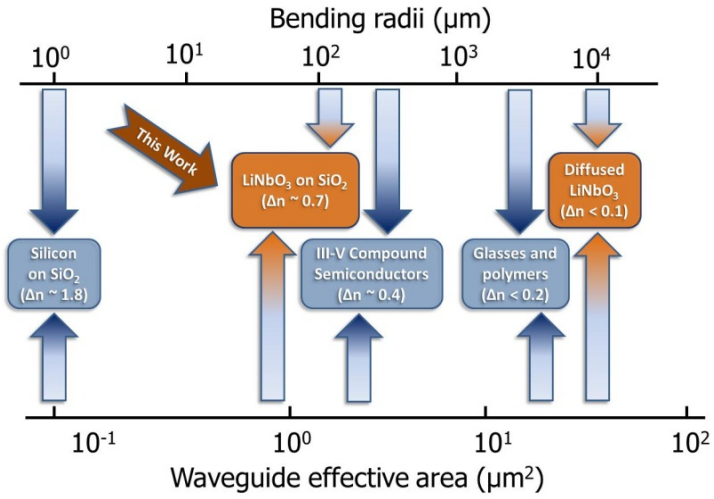

Fig. 1. Typical ranges of effective areas and minimum radii for negligible (< ~0.1 dB) bending loss at 90° bends are shown for different waveguides technologies. Δn denotes the rough refractive index contrast between core and cladding of the waveguides.

2. The novel device concept and fabrication method

Conventional $LiNbO_3$ waveguides are typically made by diffusion or proton-exchange methods [14,15]. Here, a novel technology that can realize much more compact $LiNbO_3$ devices on silicon substrates is introduced. It is estimated that the waveguide core size and bending radius of $LiNbO_3$ devices can be reduced by one to two orders of magnitude using this technology, as summarized in Fig. 1.

The novel platform on silicon substrates is schematically shown in Fig. 2. The waveguide structure consists of a thin layer of $LiNbO_3$ core region, a silicon dioxide (SiO_2) bottom cladding, and a tantalum pentoxide (Ta_2O_5) rib region loaded on top of the $LiNbO_3$ layer for

#196230 - $15.00 USD Received 22 Aug 2013; revised 7 Oct 2013; accepted 8 Oct 2013; published 18 Oct 2013

ridge formation. It is noted that, ignoring the birefringence of $LiNbO_3$, the refractive index of Ta_2O_5 is close to that of $LiNbO_3$. Hence, a ridge waveguide can be effectively formed, while the difficulties of directly etching $LiNbO_3$ are avoided. Also, the platform uses submicron layers of $LiNbO_3$ and Ta_2O_5, which allows creation of high-index contrast optical waveguides with low bending loss on silicon substrates with $LiNbO_3$ as the active region. It is noteworthy that recently thin layers of $LiNbO_3$ have been successfully bonded on top of standard SOI photonic devices [16–18]. However, since it is the evanescent tail of the optical mode of silicon waveguides that overlaps the $LiNbO_3$ cladding layer, the efficiency of the effective EO effect in these devices is low.

To demonstrate the devices schematically shown in Fig. 2, thin films of $LiNbO_3$ on silicon substrates are needed. Crystal ion slicing has been used for fabrication of thin films of silicon on silicon substrates in the past. That is the silicon-on-insulator (SOI) wafers, which are widely used for silicon photonic devices and circuits [1]. The first author and colleagues have previously demonstrated that a similar technique can be used for fabrication of thin films of $LiNbO_3$ on $LiNbO_3$ substrates [19,20]. It was shown that the optical properties of the crystals were preserved in the process and optical waveguides and modulators in submicron thin films of $LiNbO_3$ are feasible [21].

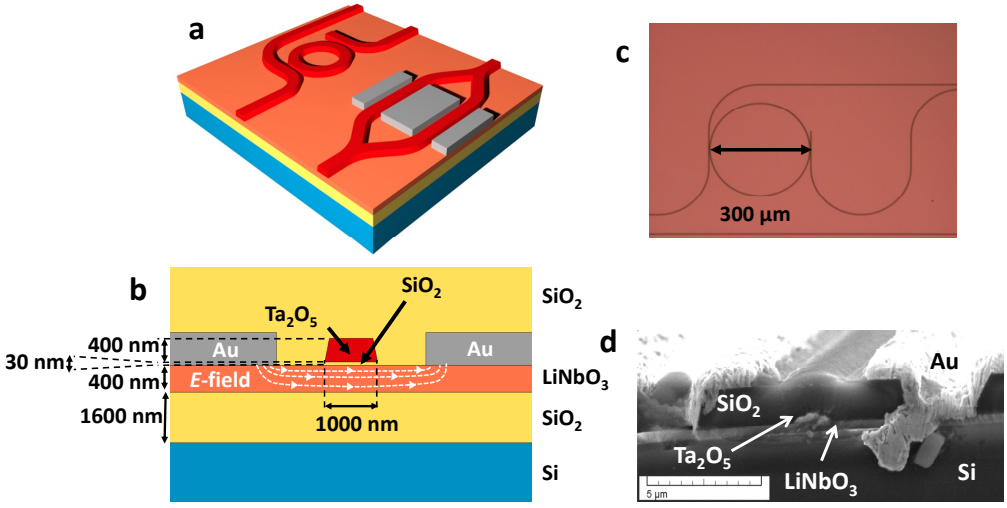

Fig. 2. (a) Schematics of the demonstrated microring resonators and Mach-Zehnder modulators are shown. The top SiO_2 cladding layer and the ultrathin SiO_2 diffusion barrier shown in (b) are omitted here for simplification. The dimensions are not in scale; (b) Cross-section of the waveguide structure at one arm of the modulator with typical dimensions. The different layers are Si (substrate), SiO_2 (claddings and diffusion barrier regions), $LiNbO_3$ (core and active region), Ta_2O_5 (loaded rib), Au (metallic contact). Shown also is a simplistic RF electric-field profile in the $LiNbO_3$ active region; (c) Top-view high-magnification optical microscope image of a fabricated ring-resonator with input and output bent bus waveguides; (d) SEM image of cross-section of a fabricated waveguide.

Since then, significant improvements in bonding techniques allow bonding at room temperature. Thus, fabrication of thin films of $LiNbO_3$ on silicon substrates is possible, as the difficulties of cracking that exists at elevated temperatures (due to different thermal expansion coefficients between silicon and $LiNbO_3$) are avoided.

The processing steps proposed and demonstrated here are summarized in Fig. 3. The highly repeatable and reliable process proposed here uses ion implantation and room-temperature wafer bonding to transfer a thin layer of $LiNbO_3$ to a silicon substrate coated with a thermally-grown SiO_2 buffer (cladding) layer. After the room-temperature initial bonding, a thermal process at 200°C is employed to not only slice the $LiNbO_3$ wafer at the peak position

#196230 - $15.00 USD Received 22 Aug 2013; revised 7 Oct 2013; accepted 8 Oct 2013; published 18 Oct 2013

of the implanted ions but also to improve the formed bonding. Chemical-mechanical polishing (CMP) is applied on the films in order to achieve the smooth surfaces needed for high-quality optical waveguides. Figure 3(e) shows an image of a 3" thin film of bonded $LiNbO_3$ to a 4" silicon wafer with no evidence of cracking or other bonding issues.

Using silicon substrate is not only important for future integration with silicon electronics and photonics, but also significantly simplifies the processing of $LiNbO_3$ devices. For example, it is well-known that, due to extremely low thermal conductivity of $LiNbO_3$ and extremely high level of pyroelectric charges, thermal cycling of the material is very difficult. Silicon, on the other hand, is a very versatile material for processing. It can easily go through temperature cycling without any problem. Hence, various processing steps can be performed easily. Also, since the volume of the $LiNbO_3$ thin film is very small, the formation of pyroelectric charges does not cause sparking.

Attaining the discussed thin films of $LiNbO_3$ is critical for vertical optical confinement in submicron waveguides. For lateral confinement in the waveguides, an etching technique may be employed. However, etching $LiNbO_3$ is very hard and it might be impossible to achieve the ultralow surface roughness required for low-loss waveguides. Ion beam milling [21–23], and wet etching [24] are some of the techniques pursued for achieving $LiNbO_3$ ridge waveguides. The latter technique has been more successful in achieving reasonably low-loss waveguides [24]. However, non-vertical sidewalls, low etch rates and undercutting are common issues of wet etching recipes. As a result, the waveguide widths are typically several microns and hence tightly-confined submicron waveguides cannot be achieved. Also, accurate control of small feature sizes, like the submicron gaps required for coupling in and out of microring resonators, is hardly possible by wet etching.

We have recently developed a novel method for fabrication of nanophotonic devices in Ta_2O_5 using selective oxidation of the refractory metal (SORM), tantalum (Ta) [25]. We have shown that this method eliminates the surface roughness and also allows fabrication of Ta_2O_5 waveguides and couplers with submicron gaps easily [25]. As mentioned, Ta_2O_5 has a refractive index roughly matched to that of $LiNbO_3$ and hence it can be used as a rib-loaded layer in combination with a $LiNbO_3$ slab layer to form a composite ridge waveguide (see Fig. 2).

In the demonstrated fabrication process, first, an ultrathin (30 nm) layer of SiO_2 is deposited on $LiNbO_3$-on-Si wafers as a diffusion barrier to prevent out-diffusion of oxygen from $LiNbO_3$ in the Ta oxidation step (COMSOL^{TM} simulations confirm that the existence of this ultrathin SiO_2 layer does not disturb the optical mode of the waveguides). Then, Ta is deposited on $LiNbO_3$ thin films that are prepared by the explained crystal ion slicing method. A plasma-enhanced chemical vapor deposition (PECVD) SiO_2 mask is then patterned on tantalum by lithographic techniques for selective oxidation of Ta at 520°C. After oxidation, a composite rib-loaded waveguide is formed consisting of Ta_2O_5 ridge layer and $LiNbO_3$ slab layer. The mask layer is subsequently removed, the remaining non-oxidized tantalum layer is dry-etched by a chlorine-based recipe, and the device is covered with SiO_2 or other materials for passivation. In the next step, the top cladding layer is etched and metal electrodes are deposited or electroplated to form a final device structure using standard fabrication techniques. Oxidation of Ta to form Ta_2O_5 could cause stress, which is disadvantageous for processing. However, since the waveguide width are very narrow, the oxidation step does not create wafer bending as might be anticipated. Figure 2(d) shows a scanning electron microscopy (SEM) image of a fabricated optical modulator.

#196230 - $15.00 USD Received 22 Aug 2013; revised 7 Oct 2013; accepted 8 Oct 2013; published 18 Oct 2013

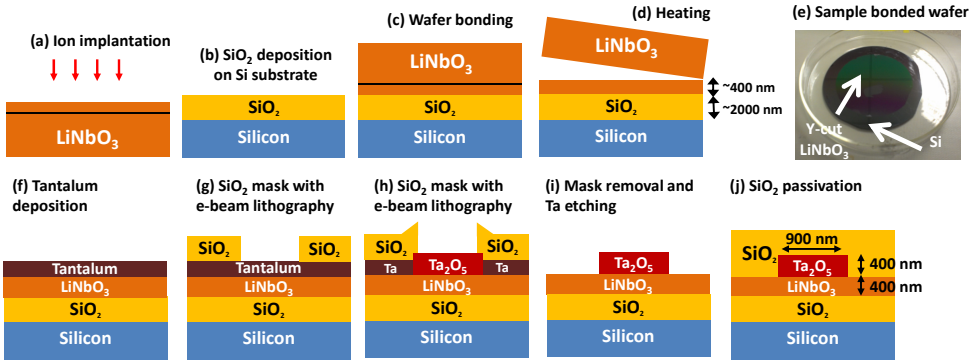

Fig. 3. (a)-(d) Process steps for the fabrication of $LiNbO_3$-on-Si wafers; (e) Picture of successful bonding of a 3-inch Y-cut $LiNbO_3$ wafer bonded to a 4-inch silicon wafer; (f)-(j)The proposed process steps of selective oxidation of tantalum to form submicron $LiNbO_3$ ridge waveguide on silicon.

3. Design of prototype devices

Having established the fabrication process described in the previous section, optical waveguides, Mach-Zehnder modulators and microring resonators were designed. A refractive index value of 2.1 to 2.2 for Ta_2O_5 layers were measured in the 1550 nm range by ellipsometry techniques. It is noted that the dispersion properties of Ta_2O_5 is dependent on the preparation method, as reviewed elsewhere [26]. For future applications, such as nonlinear optical effect that require phase-matching, the material dispersion of Ta_2O_5 versus $LiNbO_3$ must be carefully accounted for in the waveguide design. Nonetheless, for the present demonstration, as long as the indices of the two materials at 1,550 nm are within ± 0.1 of each other the waveguides can be properly designed according to our COMSOL simulations.

In order to achieve small bending radii using this geometry for telecommunication wavelengths, slab layers of ~400 nm thickness with rib height of ~200-400 nm are required (see Fig. 2(b)). Figure 4(a) shows the calculated optical mode for a 200-nm-tall, 1-μm-wide Ta_2O_5 rib on a 400-nm $LiNbO_3$ slab layer with 4-μm gap between the electrodes shown in white. Calculation results using COMSOL™ show negligible bending loss for devices with bending radius of approximately 100 μm for this structure. Bending radius of 50 μm is also possible using a 300-nm $LiNbO_3$ slab height. Further reduction of bending radius is possible at the expense of lower confinement of the optical mode and less power overlap with the $LiNbO_3$ slab region. As can be seen in Fig. 4(a), the optical mode is confined to an area of approximately less than 1 μm by 2 μm. This is smaller, by at least an order of magnitude, compared to diffusion-based devices. Hence, it is expected that highly efficient nonlinear optical devices become practical using our proposed approach.

Another advantage of the highly-confined optical waveguides is that it is possible to place the metallic electrodes in much closer proximity of the waveguides without introducing metallic optical absorption. This leads to a lower voltage to attain the same radio-frequency (RF) electric field for EO modulation. Calculations show that the gap between the electrodes can be as small as 4 μm in this structure without significant absorption of light by the electrodes. This is smaller by a factor of 5 compared to conventional $LiNbO_3$ devices. As can be seen in Fig. 4(a), there is negligible optical power close to the metallic electrodes with 4 μm gap in between. The crystalline orientation of the $LiNbO_3$ layer can be chosen to be *Y*- or *X*-cut, since in either case, electrodes can be conveniently placed laterally and an electric field along the *Z*-axis can be applied to the nonlinear material for EO modulation. In this work, *Y*-cut $LiNbO_3$ was chosen. Figure 4(b) shows the calculated RF field for the modulator by applying 1 V of bias to the electrodes. Also, the electrodes are in direct contact with the $LiNbO_3$ thin film layer. This design eliminates the problem of weak electric field previously

#196230 - $15.00 USD Received 22 Aug 2013; revised 7 Oct 2013; accepted 8 Oct 2013; published 18 Oct 2013

reported in the $LiNbO_3$ region in *Z*-cut thin-film devices [21] due to very large dielectric constant difference that exists between SiO_2 and $LiNbO_3$. As can be seen in Fig. 4(b), the resulting electric field is approximately 2×10^5 V/m, which is close to the value of 2.5×10^5 V/m, that is, when uniform electric field with a gap of 4 μm is assumed. The estimated half-wave voltage, $V_\pi.L$, of this design is 1.5 V.cm, which is about 10 times lower than commercially available devices.

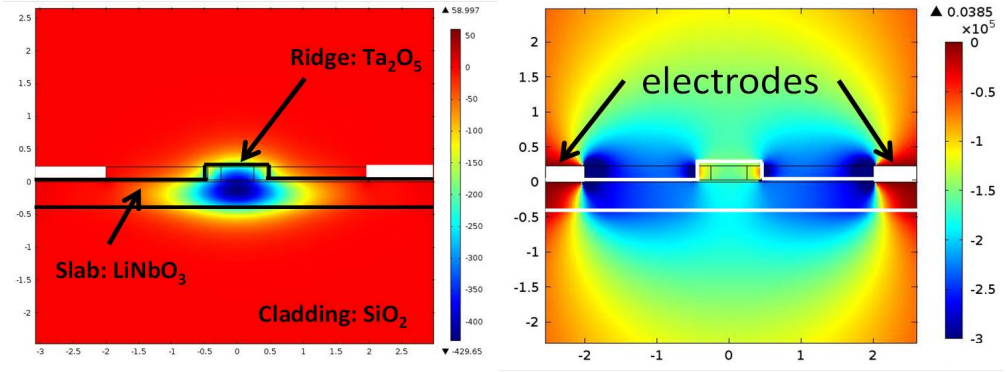

Fig. 4. (a) Calculated optical mode profile with 400-nm-thick lithium niobate and 200-nm-tall, 1-μm-wide tantalum pentoxide ridge waveguide; (b) Calculated RF mode profile with 4 μm gap between electrodes. High confinement allows short gaps between electrodes without introducing absorption loss.

4. Performance of demonstrated prototype devices

As a first demonstration of a photonic device using this technology, microring resonators were considered. Microring resonators have a wide range of photonic applications and are also ideal for accurate measurement of waveguide propagation losses. Resonators with high quality factor, *Q*, have been demonstrated in silicon and other materials, such as polymers and glass [27–30]. It is possible to achieve ultracompact EO modulators using microring resonators, as demonstrated first on polymers [30]. Using thin films of $LiNbO_3$ bonded to $LiNbO_3$ substrates by an adhesive polymer, and by employing ion milling for etching the waveguides, and very low *Q* microring resonators have been demonstrated in the past [23]. Here, much higher *Q* values and relatively low-loss waveguides are reported on the proposed platform, as follows.

Microresonators with two coupled waveguides were fabricated as shown in Fig. 2(a) and 2(c) in our proposed platform. Several devices with different diameters and coupling gaps were designed and fabricated. Curved input-output waveguides (buses) were used to study the impact of bending and the microresonator on the optical transmission as a function of wavelength. The coupling and bending losses were calculated and designed using finite element modeling tools. Figure 2(c) shows an image of a fabricated photonic circuit with a ring radius of 150 μm. The devices were characterized using a tunable semiconductor laser. Light was coupled into the chips by a lensed fiber and coupled out via an objective lens into a low-speed photodetector. Standard micromanipulator stages were used for manual alignment. Figure 5(a) presents the measured transverse-electric (TE) mode transmission spectrum of a fabricated microresonator, with 150 μm radius, in the vicinity of the 1550-nm telecommunication wavelength range. The bending loss for this radius is negligible as was discussed in designs of Section 3. The estimated unloaded *Q* obtained by curve fitting [30] is ~7.2×10^4 and the unloaded finesse is 50. The extracted propagation loss is 5 dB/cm. The loaded *Q* of the device presented in Fig. 5(a) is 4.5×10^4, which is over an order of magnitude higher than previous results [23]. The somewhat high value of loss could be due to material

#196230 - $15.00 USD Received 22 Aug 2013; revised 7 Oct 2013; accepted 8 Oct 2013; published 18 Oct 2013

absorption or scattering of light in the Ta_2O_5 ridge region, as we have seen in Ta_2O_5 waveguides on silicon too [25]. One possible explanation is that during deposition of the Ta layer, there is a high percentage impurities in Ta and hence the loss is attributed to this impurity in the rib layer. Another possible explanation is that Ta_2O_5 is prone to polycrystalline forms with α- and β-phases, whose grain boundaries can lead to scattering loss. Further investigation of these and other possible causes is underway.

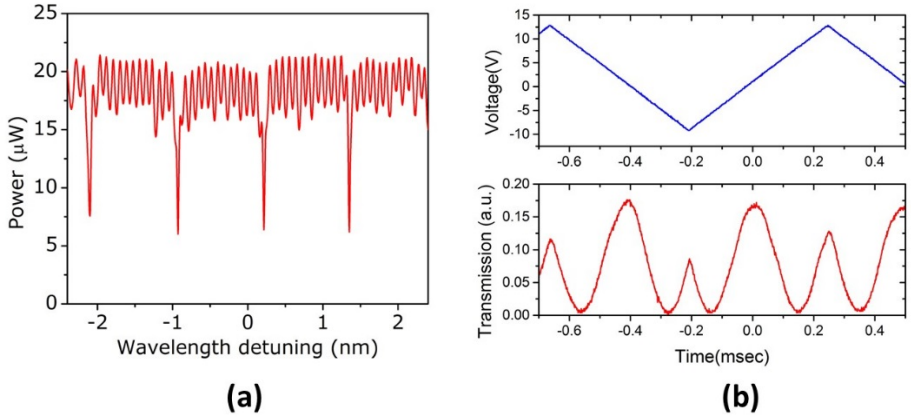

Fig. 5. (a) Transmission spectrum of a microresonator with 300 μm diameter for the TE mode around 1550 nm wavelength. The resonance linewidth is 2.7 GHz; (b) Applied sawtooth electrical signal and the measured modulation response of a 6-mm-long Mach-Zehnder modulator. The measured V_π is 6.8 V.

To demonstrate improvement in the functionality of a widely used active device using this technology, Mach-Zehnder modulators consisting of two *Y*-junctions and two straight 6-mm-long arms were designed and fabricated on *Y*-cut thin films. Push-pull electrodes were utilized, as shown in Fig. 2(a). The gold (Au) electrodes were deposited and patterned by standard lithographic techniques to achieve the final structure shown in the SEM image of Fig. 2(d). The devices were characterized by applying a sawtooth modulation voltage around 1 kHz using the same setup as discussed above. It was confirmed that no current flows through the electrodes, as expected from the dielectric nature of SiO_2 and $LiNbO_3$. Figure 5(b) shows the applied low-frequency electrical signal and the measured optical modulation signal for a device with 7 μm gap between the electrodes.

As can be seen in Fig. 5(b), the V_π of the device is 6.8 V. Since the electrodes are 6 mm long, the measured half-wave voltage-length product, $V_\pi.L$, is equal to ~4 V.cm. This record value of $V_\pi.L$ for $LiNbO_3$ is lower, by at least a factor of 3, than the best optimized diffusion-based modulators [31]. The simulated value of $V_\pi.L$ (using the EO coefficient, r_{33}, of $LiNbO_3$ single crystals) is ~4.1 V.cm for this device (this is higher than the aforementioned value of 1.5 V.cm because of larger gap between the electrodes and slightly thicker Ta_2O_5 layer used in the fabricated devices compared to the simulations of Section 3). The agreement between experimental and simulated value of $V_\pi.L$ indicates that the extracted value of r_{33} is approximately 31 pm/V, which is very close that of $LiNbO_3$ single crystals. This means that the crystalline quality of the $LiNbO_3$ layers is not degraded after annealing the ion implanted thin films.

When the transmission in Fig. 5(b) is plotted in logarithmic scale, an extinction ratio (ER) of approximately 20 dB is measured in the modulator. This high ER value, possible through the EO effect, is a clear advantage over silicon optical modulators, based on free-carrier plasma effect, which typically suffer from low ER in the modulation response [32]. Also, a fit to the results of Fig. 5(b) confirms that the response is sinusoidal, as expected in a Mach-

#196230 - $15.00 USD Received 22 Aug 2013; revised 7 Oct 2013; accepted 8 Oct 2013; published 18 Oct 2013

Zehnder-type device. The fit error is less than 3% with respect to the applied sawtooth voltage.

As was discussed in Section 3, with more optimized design, smaller electrode gaps and higher fabrication tolerances, it is predicted that $V_{\pi}.L$ as low as 1.5 V.cm is feasible, which will be approximately 10 times lower than the state of the art. By combining this reduction in $V_{\pi}.L$ of the device with folded-waveguide schemes, which can become possible for the first time in $LiNbO_3$, it will be then practical to reduce the footprint of $LiNbO_3$ Mach-Zehnder optical modulators by two orders of magnitude to less than 0.5 mm × 0.5 mm and achieve a V_{π} of ~1 V.

The high-speed modulation properties of the device using non-RF-terminated electrodes were also measured using a network analyzer. The devices are certainly functional up to several GHz according to the measured S_{21} parameter of the modulated signal. However, full characterization of the modulation properties and extraction of the modulation bandwidth requires careful design and fabrication of devices with travelling-wave electrodes and RF termination, which is beyond the scope of this work.

5. Conclusions

In conclusion, the present work demonstrates a novel integrated photonic platform based on thin films of $LiNbO_3$ on silicon substrates fabricated by room-temperature bonding and SORM methods. The platform allows significantly improved performance for various photonic devices based on $LiNbO_3$. Here, improvements for a typical passive optical device (microring resonators) and a typical active device (optical modulators) are reported. It is expected that high-performance nonlinear devices for second-harmonic generation, parametric amplification, and entangled photon generation can be attained on the platform in the future.

Acknowledgment

The work is being supported by the U.S. Office of Naval Research (ONR) Young Investigator Program (YIP) under the Grant Number 11296285.

#196230 - $15.00 USD Received 22 Aug 2013; revised 7 Oct 2013; accepted 8 Oct 2013; published 18 Oct 2013